Suzaku observations of Markarian 335: evidence for a distributed reflector

J. Larsson,[1][*] G. Miniutti,[1] A. C. Fabian,[1] J. M. Miller,[2] C. S. Reynolds[3] and G. Ponti[4,5]

[1]*Institute of Astronomy, University of Cambridge, Madingley Road, Cambridge CB3 0HA*
[2]*Department of Astronomy and Astrophysics, The University of Michigan, 500 Church Street, Ann Arbor, MI 48109, USA*
[3]*Department of Astronomy, University of Maryland, College Park, MD 20742, USA*
[4]*Dipartimento di Astronomia dell' Universitá degli Studi di Bologna, via Ranzani I, I-40127 Bologna, Italy*
[5]*IASF/INAF Sezione di Bologna, via Gobetti 101, I-40129 Bologna, Italy*

ABSTRACT

We report on a 151-ks net exposure *Suzaku* observation of the narrow-line Seyfert 1 galaxy Mrk 335. The 0.5–40 keV spectrum contains a broad Fe line, a strong soft excess below about 2 keV and a Compton hump around 20–30 keV. We find that a model consisting of a power law and two reflectors provides the best fit to the time-averaged spectrum. In this model, an ionized, heavily blurred, inner reflector produces most of the soft excess, while an almost neutral outer reflector (outside $\sim 40r_{\rm g}$) produces most of the Fe line emission. The spectral variability of the observation is characterized by spectral hardening at very low count rates. In terms of our power-law + two-reflector model it seems like this hardening is mainly caused by pivoting of the power law. The rms spectrum of the entire observation has the curved shape commonly observed in active galactic nuclei, although the shape is significantly flatter when an interval which does not contain any deep dip in the light curve is considered. We also examine a previous 133-ks *XMM–Newton* observation of Mrk 335. We find that the *XMM–Newton* spectrum can be fitted with a similar two-reflector model as the *Suzaku* data and we confirm that the rms spectrum of the observation is flat. The flat rms spectra, as well as the high-energy data from the *Suzaku* PIN detector, disfavour an absorption origin for the soft excess in Mrk 335.

Key words: galaxies: active – galaxies: Seyfert – galaxies: individual: Mrk 335 – X-rays: galaxies.

1 INTRODUCTION

The X-ray spectra of type 1 active galactic nuclei (AGN) are usually dominated by a power-law component. They also often exhibit a broad, skewed Fe line around 6 keV, as well as smooth component rising above the power-law continuum below about 2 keV, the so-called soft excess. While it is well established that the broad Fe line arises due to reflection of the continuum power law in the inner accretion disc (where it is broadened by Doppler and relativistic effects), the origin of the soft excess remains a question of much debate.

The soft excess has a very similar spectral shape in AGN covering several decades in mass (Gierliński & Done 2004; Crummy et al. 2006), suggesting that its origin is in atomic rather than thermal processes. An obvious candidate of atomic origin is the reflection spectrum associated with the broad Fe line. In this model, the soft excess is due to the blurring of soft emission lines from the inner parts of the accretion disc. The reflection model has been applied

successfully in a number of AGN (e.g. Crummy et al. 2006), although sources that exhibit a strong soft excess but no broad Fe line are difficult to explain in this model (see e.g. Brenneman et al. 2007). Another proposed explanation for the soft excess is that it is due to smeared absorption by optically thin material in the line of sight (Gierliński & Done 2004). This model has been seen to provide equally good fits as the reflection model (e.g. Middleton, Done & Gierliński 2007). However, the model used in these fits has been very simplistic, ignoring emission resulting from the absorber and the acceleration of the matter. A more realistic absorption model does not reproduce the smooth shape of observed soft excesses unless extreme velocities are incorporated (Schurch & Done 2007).

Mrk 335, also known as PG 0003+199, is a narrow-line Seyfert 1 (NLS1) galaxy at redshift $z = 0.026$. It exhibits both a strong soft excess and a broad Fe line. Unlike most Seyfert 1 galaxies, it does not show any clear signs of complex, warm absorption at low energies, making it an ideal target for studying the origin of the soft excess.

The soft excess in Mrk 335 was first observed by *EXOSAT* (Pounds et al. 1987; Turner & Pounds 1988) and was later confirmed by *BBXRT* (Turner et al. 1993). No significant absorption

[*]E-mail: jlarsson@ast.cam.ac.uk

edges were detected in the *BBXRT* observation but an Fe edge in *Ginga* data lead Turner et al. (1993) to suggest the presence of a variable, ionized absorber. A subsequent *ASCA* observation again revealed the presence of a strong soft excess, but showed no clear evidence of edges or ionized absorption at low energies (Reynolds 1997; George et al. 1998). The *ASCA* spectrum also showed evidence for a broad Fe line (Nandra et al. 1997) and Ballantyne, Iwasawa & Fabian (2001) found a good fit to the entire 0.6–10 keV band with an ionized reflection model. *BeppoSAX* data (Bianchi et al. 2001) clearly showed a broad Fe line as well as a soft excess, but revealed a rather small Compton reflection component.

XMM–Newton observed Mrk 335 for the first time in 2000. The observation was first analysed by Gondoin et al. (2002), who favour a model in which the soft excess consists of a combination of bremsstrahlung emission and ionized reflection from the accretion disc. No absorption edges apart from the 0.54-keV edge due to Galactic oxygen were seen in the RGS spectrometer.

The *XMM–Newton* observation was later reanalysed by Longinotti et al. (2007), who detected a narrow absorption feature at 5.9 keV, which, if it is identified with Fe XXVI, is inflowing at ∼0.11–0.15c, or, if at rest, is located close to the black hole and gravitationally redshifted. Both Crummy et al. (2006) and Middleton et al. (2007) have also fitted the *XMM–Newton* data as a part of a sample of type 1 AGN. Crummy et al. (2006) find that the spectrum can be well fitted with a reflection model, while Middleton et al. (2007) show that an equally good fit can be obtained if the soft excess is modelled as smeared absorption.

In 2006 January, *XMM–Newton* re-observed Mrk 335 for 133 ks. In addition to a strong soft excess below 2 keV, this observation revealed a double-peaked Fe emission feature with peaks at 6.4 and 7 keV (O'Neill et al. 2007). Spectral fitting of this feature suggested that a moderately broad relativistic line is present but that the two peaks are due to narrow lines originating in more distant material. The authors further note that the reflection model inferred from the data above 3 keV still leaves a soft excess when extrapolated to lower energies. The rms variability spectrum of the observation is consistent with being constant, disfavouring the absorption model for the soft excess, which, assuming that the ionization state of the absorber is driven by the continuum variability, predicts enhanced variability at low energies (Gierliński & Done 2006).

Recent *Swift* observations of Mrk 335, carried out in 2007 May and June/July, caught the source in an extremely low state, with the flux having diminished by a factor of 30 compared to previous observations. In this low state the source exhibited a very hard spectrum above 2 keV as well as a soft excess at low energies. The spectral changes together with the sudden drop in flux have been interpreted in terms of a partial covering model (Grupe, Komossa & Gallo 2007) as well as in a reflection model (Gallo et al., in preparation).

In this paper we present the results of a 316-ks (∼150 ks net exposure) *Suzaku* observation of Mrk 335 performed in 2006 June. This observation was carried out before the sudden drop in flux mentioned above and caught the source in its typical flux state. We also analyse the 133-ks *XMM–Newton* observation performed in 2006 January.

This paper is organized as follows. Section 2 describes the observations and the data reduction, Sections 3 and 4 describe the spectral analysis of the *Suzaku* and *XMM–Newton* time-averaged spectra, and the spectral variability of both observations is presented in Section 5. Section 6 contains a discussion of the results, and a summary is given in Section 7.

2 OBSERVATIONS AND DATA REDUCTION

2.1 The *Suzaku* observation

Mrk 335 was observed by *Suzaku* between 2006 June 21 and 24 for a total duration of 316 ks. Event files from version 1.2.2.3 of the *Suzaku* pipeline processing were used and spectra were extracted using XSELECT.

The net exposure time of all four XIS detectors is 151 ks. For each XIS, source spectra were extracted from circular regions of 4.3 arcmin radius centred on the source (which was observed off-axis in the HXD nominal position). Background spectra were extracted from two circular regions with the same total area as the source region, avoiding the chip corners with the calibration sources. Response matrices and ancillary response files were generated for each XIS using XISRMFGEN and XISSIMARFGEN version 2006-11-26. The ARF generator should account for the hydrocarbon contamination on the optical blocking filter (Ishisaki et al. 2007).

The source count rates over the 0.7–10 keV energy range for the three front-illuminated (FI) detectors are 1.299 ± 0.003 counts s^{-1}(XIS0), 1.484 ± 0.003 counts s^{-1} (XIS2) and 1.364 ± 0.003 counts s^{-1} (XIS3). The back-illuminated (BI) detector (XIS1) has a count rate of 2.243 ± 0.004 counts s^{-1} in the 0.3–8 keV band. The background typically contributes 2–3 per cent of the total count rate for all four detectors.

At the time of our observation, the bias voltage for 16 of the 64 HXD PIN diodes had been reduced from 500 to 400 V, in order to suppress a rapid increase of noise events. The PIN event file was therefore filtered to exclude the diodes biased with 400 V, and the corresponding response file (ae_hxd_pinhxnom123_20060814.rsp) was used. A model for the non-X-ray background was provided by the HXD team. Source and background spectra were constructed from identical good time intervals and the exposure time of the background spectrum was increased by a factor of 10 (to account for the fact that the background model was generated with 10 times the actual count rate in order to minimize the photon noise). After dead-time correction the net exposure time of the PIN was 120 ks.

The total PIN count rate over the 14–40 keV energy range is 0.296 ± 0.002 counts s^{-1}, compared to 0.262 ± 0.005 counts s^{-1} for the background. Since the background is so much higher than the source, the accuracy of the background model is very important for our results. We therefore compared the background model to the night earth spectrum, which was obtained by selecting periods of earth occultation during the observation. Since the earth is dark in the hard X-rays the background model should agree with the night earth spectrum. We find that that the background model overpredicts the night earth data by about 6 per cent, but that the spectral shape is well reproduced. We can therefore simply correct the count rate of the background model so that it matches the night earth data when fitting the time-averaged spectrum. Investigations of the background model on shorter time-scales unfortunately show that the systematic uncertainties of the model are too large for timing analysis to be carried out, and we therefore defer this analysis to a later time when a more accurate background model will be available.

Since the background model discussed above does not include the contribution from the cosmic X-ray background (CXB), a spectral model for it is included in all the fits. The model, which has the form $2.06 \times 10^{-6}(E/100\,\text{keV})^{-1.29} \exp(-E/41.13\,\text{keV})$, is based on the HEAO-A1 spectrum and has been renormalized to the HXD field of view. The CXB flux over the 14–40 keV band predicted by this model represents about 25 per cent of the source flux.

2.2 The *XMM–Newton* observation

XMM–Newton observed Mrk 335 between 2006 January 03 and 05 for a total duration of 133 ks (observation ID 0306870101). The data were reduced using the *XMM–Newton* Science Analysis System version 7.0.0. We use only the data from the EPIC pn camera, which was operated in the small window mode during the observation. Because of the small window mode the data are not affected by photon pile-up. The source spectrum was extracted from a circular region of radius 34 arcsec centred on the source, and the background spectrum was extracted from two circular regions with a total area three times that of the source region. Inspection of the background showed that strong flaring was present at the beginning and at the end of the observation. Excluding these time intervals leaves a total good exposure time of 115 ks.

3 THE TIME-AVERAGED *Suzaku* SPECTRUM

In order to investigate the agreement between the four XIS detectors we initially fitted them separately with a simple power-law model. The three FI XIS showed very similar spectra over the 0.7–10 keV energy range, with the photon indices agreeing to within 0.01. Larger differences are seen below 0.7 keV and the agreement becomes very poor below about 0.6 keV (see e.g. Fig. 2). Since we find that including the data between 0.6 and 0.7 keV only makes the quality of the fits worse without significantly changing any of the fit parameters, we choose 0.7 keV as our lower energy limit. (We will use the BI XIS to constrain our spectral models at lower energies.) When the 0.7–10 keV FI XIS spectra were fitted simultaneously with the photon index tied, the relative normalizations were found to be XIS0/XIS2 = 0.93 and XIS3/XIS2 = 0.99. These values were also obtained when fitting more complicated models, and in all subsequent fits we will fit the FI XIS simultaneously with gamma tied. The BI XIS (XIS1) was found to have a somewhat steeper spectrum than the other XIS ($\Delta\Gamma \approx 0.1$ in the same energy range). As XIS1 also has a higher effective area at softer energies (we use the 0.3–8 keV energy range) we choose to fit it separately and use it mainly to constrain our models at very low energies. Due to calibration uncertainties near the instrumental Si K edge at 1.84 keV we always ignore 1.8–1.9 keV in the FI XIS and 1.7–1.9 keV in the BI XIS.

The PIN spectrum is unfortunately associated with uncertainties regarding the background modelling and the cross-normalization with respect to the XIS detectors. Although this means that we cannot use the PIN data to accurately constrain parameters of different spectral models, we can still use it to distinguish between models that fit the data at lower energies.

Below we will first consider the 2–10 keV spectrum and then include the low-energy data down to 0.3 keV. As a last step we will consider the 14–40 keV PIN spectrum. Throughout this paper, errors are quoted at the 90 per cent confidence level and energies of spectral features are quoted for the rest frame of the source.

3.1 The 2–10 keV spectrum

The most prominent feature in the 2–10 keV energy range is the broad Fe line which extends from about 5 to 7 keV. The line profile is shown in Fig. 1 as a ratio to a power law modified by Galactic absorption ($N_{\mathrm{H}} = 3.99 \times 10^{20}\,\mathrm{cm}^{-2}$, included in all fits from hereon), fitted over the 2–4.5 and 7.5–10 keV energy ranges. The power law has a photon index of $\Gamma = 2.09 \pm 0.02$.

In order to find a phenomenological description for the data over the whole 2–10 keV band we start by adding a Gaussian line to the
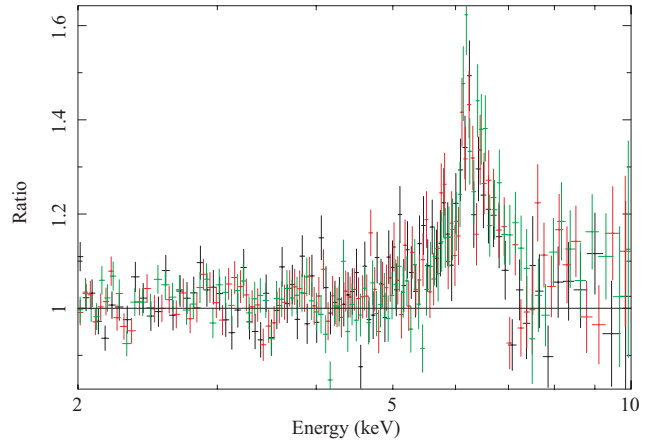

Figure 1. The *Suzaku* FI XIS spectrum shown as a ratio to a power law fitted over the 2–4.5 and 7.5–10 keV energy ranges. Data points in black, red and green correspond to XIS 0, 2 and 3.

power-law model. This simple model provides a good fit to the data with $\chi^2 = 4441$ for 4353 degrees of freedom (d.o.f.). The Gaussian line is found to have $E = 6.43 \pm 0.04$ keV, $\sigma = 0.40^{+0.05}_{-0.04}$ keV and equivalent width EW = 285 ± 34 eV. The photon index of the power law is still $\Gamma = 2.09 \pm 0.01$. When adding a narrow line around 6.4 keV to the model (to check for a narrow component of the Fe line from distant matter) the fit improves by $\Delta\chi^2 = 19$ for 2 d.o.f. The narrow line has energy $E = 6.36 \pm 0.03$ keV[1] and EW = 29 ± 14 eV. With the narrow line included, the broad-line parameters change to $E = 6.45 \pm 0.05$ keV, $\sigma = 0.47^{+0.10}_{-0.06}$ keV and EW = 250^{+40}_{-39} eV.

No other narrow lines are detected in the spectrum. In particular, we do not detect the 5.9 keV absorption line seen in the 2000 *XMM–Newton* observation (Longinotti et al. 2007) or the 7 keV emission line seen in the 2006 *XMM–Newton* observation (O'Neill et al. 2007). If the narrow line around 7 keV originates in distant material, as suggested by O'Neill et al. (2007), it seems strange that is has disappeared in the 6 months between the *XMM–Newton* and *Suzaku* observations. However, adding a line around 7 keV to our model for the *Suzaku* data does not improve the quality of the fit, and we find that the line tends to move to energies much lower than 7 keV. If we freeze the line energy at 6.97 keV (the energy of Fe XXVI Lyα) we find a line flux of $0.83^{+1.8}_{-0.8} \times 10^{-6}$ photons cm^{-2} s^{-1}, corresponding to an of EW = 6^{+15}_{-6} eV. Using the same model for the 2006 *XMM–Newton* data, we find a significantly higher line flux of $4.96^{+1.40}_{-1.82} \times 10^{-6}$ photons cm^{-2} s^{-1}. It thus seems clear that the emission line around 7 keV has disappeared or at least weakened significantly in the *Suzaku* observation.

We now move on to try and find a more realistic model for the data. The broad, skewed Fe line seen in Fig. 1 arises as the incident power law is reflected in the accretion disc, and should therefore have a reflection continuum associated with it. To model the reflection from an accretion disc we use the constant-density model REFLION by Ross & Fabian (2005). The parameters of the model are the Fe abundance, the ionization parameter ξ, the photon index of the incident power law and the normalization. In order to account for relativistic effects

---

[1] After completion of this work a new processing version of these data was released (V.2.0.6.13). With this version the energy of the narrow line is found to be $E = 6.39^{+0.02}_{-0.03}$ keV, i.e. completely consistent with the 6.4 keV Fe line. No other model parameters changed significantly with the new processing version.

in the vicinity of the black hole, this model is convolved with the relativistic blurring kernel KDBLUR, which is derived from the code by Laor (1991). The relativistic blurring parameters are the inner and outer radii of the disc (r_{in} and r_{out}), the inclination i and the emissivity index q (the emissivity follows the form $\epsilon \propto r^{-q}$, where r is the radius of emission).

In addition to the power law and the blurred reflection component, we also include the narrow Fe Kα line in our model. In all fits we fix the Fe abundance at the solar value, the emissivity index at $q = 3$ and the outer radius of the disc at $r_{out} = 400 r_g$ (where $r_g = GM/c^2$ is the gravitational radius). We find a best fit of $\chi^2/\text{d.o.f.} = 4416/4353$ with $\Gamma = 2.19 \pm 0.01, \xi = 30^{+3}_{-0}$ erg cm s^{-1} (the lowest allowed value), $i = 54^{+8}_{-6}$ ° and $r_{in} = 40^{+60}_{-20} r_g$. The parameters of the narrow line are found to be $E = 6.36 \pm 0.02$ keV and EW $= 60^{+14}_{-15}$ eV. In order to confirm these results we also fitted a model in which we replaced the blurring kernel KDBLUR with the KERRCONV model by Brenneman & Reynolds (2006). An important difference between these two models is that the KERRCONV model has the spin of the black hole as a free parameter. The KERRCONV model gives best-fitting parameters that are consistent with those reported above, and gives a best-fitting spin value of 0, as expected from the relatively large value of r_{in}.

It should be noted that the best fit presented above is not necessarily unique. Both a highly ionized disc and a high inclination make the blue peak of the Fe line bluer, and these parameters are hence somewhat degenerate. In fact, with an ionization parameter of $\xi = 2000$ erg cm s^{-1}, we find a fit of comparable quality to the one above ($\chi^2/\text{d.o.f.} = 4424/4353$) with $i = 19^{\circ +10^\circ}_{-19^\circ}, \Gamma = 2.06 \pm 0.01$ and similar parameters for the narrow line. We will hopefully be able to break this degeneracy by including the low-energy data.

3.2 The soft excess

We now include the data from the three FI XIS down to 0.7 keV (this lower energy limit is discussed at the beginning of the section), ignoring the 1.8–1.9 keV band which is affected by the instrumental Si edge. When extrapolating the best-fitting 2–10 keV models, a clear, rather smooth soft excess is visible below 2 keV, as shown in Fig. 2. The rati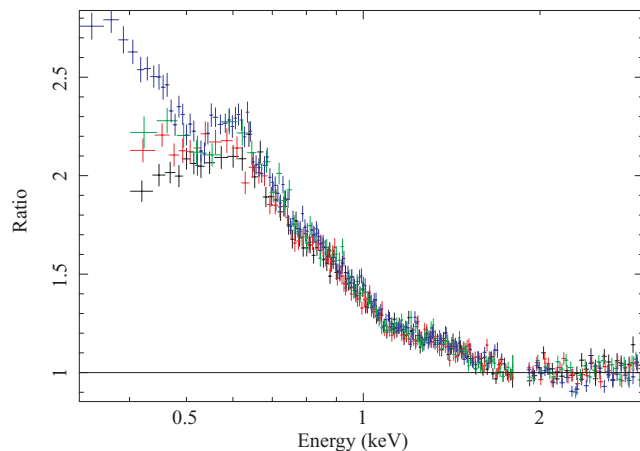o of the data to the model at 0.7 keV is 1.9 for the simple power-law model, and 1.7 and 1.5 for the highly ionized and almost neutral reflection models, respectively.

A good fit to the soft excess can be found by simply adding a blackbody component to the 2–10 keV models. A blackbody of temperature 0.13 keV together with our reflection model with $\xi = 30$ erg cm s^{-1} for instance gives χ^2 d.o.f. $= 5579/5340$. Although this solution provides a good parametrization of the data it is very unlikely to be realistic. The temperature is simply too hot for an accretion disc around a supermassive black hole, and blackbody temperatures of 0.1–0.2 keV have been found to fit soft excesses in AGN with a large range of masses and accretion rates (Gierliński & Done 2004; Crummy et al. 2006), in disagreement with the prediction that the disc temperature should scale as $T \propto M^{-1/4}(\dot{M}/\dot{M}_{Edd})^{1/4}$ (Shakura & Syunyaev 1973).

A natural explanation for the constant temperature of the soft excess is that it is due to some atomic process, and reflection is thus an obvious candidate. Since no emission lines are seen in the soft excess, this reflection has to be heavily blurred, and therefore originate in the very inner parts of the accretion disc. This poses a problem for our 2–10 keV reflection models. The inner radius of emission at $40 r_g$, as suggested by the Fe line shape, simply does not provide enough blurring to reproduce the smooth shape of the soft excess. A disc truncated at $\sim 40 r_g$ is also at odds with Mrk 335 being a high accretion rate source ($\dot{M}/\dot{M}_{Edd} = 0.79$, based on Woo & Urry 2002). It is thus possible that the disc extends further in but is unable to produce fluorescent Fe emission in the inner parts (e.g. because of its ionization state).

It seems plausible that a model with two reflectors can reproduce the data; an inner, heavily blurred reflector to produce the soft excess, and an outer reflector to produce the sharp features of the Fe line. We therefore construct a model with an inner reflector extending from 1.24 to $40 r_g$ and an outer reflector extending from 40 to $400 r_g$. If we fix the inclination at $i = 54°$ (as found for our best fit to the 2–10 keV data) we find a fit with $\chi^2/\text{d.o.f.} = 5592/5335$. This model has a photon index of $\Gamma = 2.19 \pm 0.01$ and inner and outer ionization parameters of $\xi_{in} = 310^{+10}_{-8}$ erg cm s^{-1} and $\xi_{out} = 32^{+5}_{-2}$ erg cm s^{-1}. The narrow line is found to have energy $E = 6.36 \pm 0.02$ keV and EW $= 67^{+16}_{-14}$ eV. The reflection fraction of the two reflectors is 2.8, with each of the reflectors contributing roughly the same amount. The model is plotted in Fig. 3.
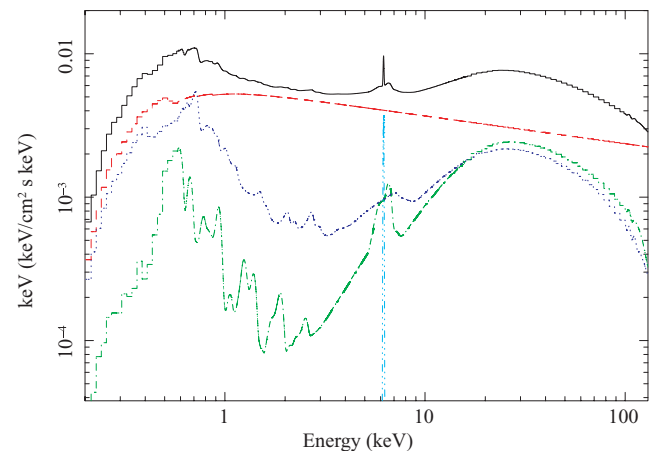

Figure 2. The *Suzaku* XIS spectrum shown as a ratio to the 2–10 keV power-law + Gaussian model, clearly revealing the soft excess. Data from the FI XIS are shown in black, red and green, and data from the BI XIS (XIS1) are shown in blue. The agreement between the detectors clearly becomes poor at low energies. The structure seen in the 0.5–0.7 keV range in XIS1 is discussed in the text.

Figure 3. Best-fitting two-reflector model for the time-averaged 0.7–10 keV *Suzaku* spectrum. The solid, black line shows the total model and the dashed, red line shows the primary power law. The inner and outer reflectors are represented by the blue, dotted line and the green, dash–dotted line, respectively. The model also includes a narrow Fe Kα line.
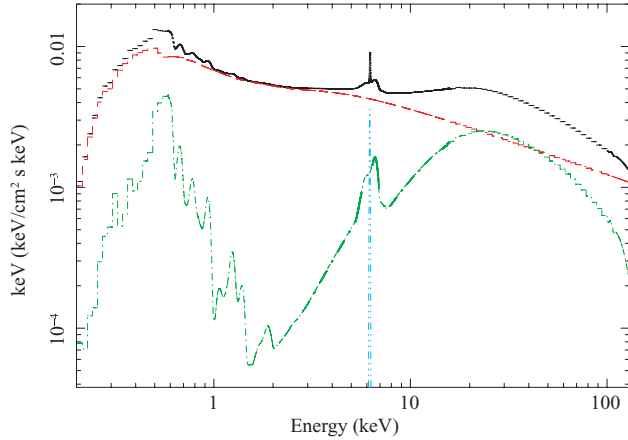
Figure 4. The best-fitting blurred absorption model for the time-averaged 0.7–10 keV *Suzaku* spectrum. The solid, black line shows the total model and the dashed, red line shows the absorbed power law. The model also includes distant reflection (green, dash–dotted line) and a narrow Fe Kα line.

It is clear that this three-component model leaves much freedom for many of the parameters and that the fit presented above is not necessarily unique. The fact that the inner disc needs to be more highly ionized than the outer one however seems robust. We were for example not able to find a satisfactory fit with a highly ionized outer reflector (together with a lower inclination) as suggested by one of our fits to the 2–10 keV data.

Another possible way of producing the soft excess is by relativistically blurred absorption of a steep continuum. Just as for the case of reflection, this model explains both the constant temperature and the smooth shape of the soft excess. In order to investigate this possibility we use the SWIND1 model of Gierliński & Done (2006). This model has three free parameters, the velocity smearing σ (assumed to be Gaussian), together with the ionization parameter and the column density of the absorbing material (ξ_a and N_H, respectively). To model the continuum we use a power law and a blurred reflection component, as the latter is still required to explain the broad Fe line. For the reflection component we use the same parameters as those found for the outer reflector in the two-reflector model, leaving only the normalization as a free parameter. We find a fit of comparable quality as the two-reflector model (χ^2/d.o.f. = 5581/5334 with $\xi_a = 499^{+53}_{-54}\,\mathrm{erg\,cm\,s^{-1}}$, $N_H = 7.4 \pm 0.9 \times 10^{22}\,\mathrm{cm^{-2}}$, $\sigma = 0.50_{-0.02}c$ (highest allowed value) and $\Gamma = 2.47^{+0.01}_{-0.02}$. The model is shown in Fig. 4.

The fact that the soft excess can be equally well fitted with smeared absorption as with blurred reflection from an accretion disc is commonly observed in AGN (e.g. Middleton et al. 2007). However, the velocity smearing of $0.5c$ that we find in our best fit with the absorption model is unreasonably high. It should also be noted that the SWIND1 absorption model is rather simplistic in its treatment of the velocity field (assumed to be Gaussian) and in that it does not include any emission from the absorbing material. It has been shown that when these issues are addressed, the model spectra include sharp features which contrast strongly with the observed smooth shapes of soft excesses (Schurch & Done 2007). We therefore favour the two-reflector model presented above as an explanation for the soft excess in Mrk 335.

3.2.1 The spectrum from the back-illuminated XIS1 detector

For XIS1, we use the 0.3–8 keV energy band, ignoring the 1.7–1.9 keV range due to the effects of instrumental Si. Since the calibration of XIS1 is still somewhat uncertain we start by comparing its low-energy spectrum with that from the long *XMM–Newton* observation. When taking the ratio of the two data sets, clear, sharp differences can be seen at low energies. The structure seen in the 0.5–0.7 keV range in Fig. 2 is, for instance, not present in the *XMM–Newton* data. As it is quite likely that at least some of these differences are due to calibration uncertainties in XIS1, we will only very briefly discuss the XIS1 spectrum.

The two-reflector model provides a good fit to the XIS1 data down to 0.5 keV (χ^2/d.o.f. = 1614/1605), with none of the parameters changing significantly from the values presented above. Extrapolation of the model down to 0.3 keV however reveals a soft excess as well as the very sharp edge around 0.5 keV. In order to fit these features with the two-reflector model we need to add an edge at 0.49 keV, and allow for a steeper emissivity profile ($q = 6.5$) as well as a steeper power law ($\Gamma = 2.29$). If the 0.49-keV edge is intrinsic to the source it can be identifies with C VI, although it seems more likely that it is an effect of inaccurate modelling of the contamination in XIS1.

3.3 The 14–40 keV PIN spectrum

In addition to a soft excess and a broad Fe line, reflection from an accretion disc should produce a Compton hump around 20–30 keV, as seen in Fig. 3. Data at these energies, provided by the *Suzaku* HXD PIN detector, are therefore crucial for testing the models derived from the XIS data. Specifically, the two-reflector model predicts about 1.4 times more flux in the 14–40 keV range than the smeared absorption model.

Mrk 335 is detected in the PIN up to about 40 keV and we stress that this detection is robust against uncertainties in the background model. However, since the background dominates the spectrum, the accuracy of the background modelling is very important for our results. As mentioned in Section 2, comparison of the instrumental background model with night earth spectra shows that the background model is overestimated by about 6 per cent. We therefore correct for this before fitting the spectrum. We also include a model for the CXB as described in the same section. The 14–40 keV flux from the CXB model represents about 25 per cent of the source flux. The cross-normalization of the PIN with respect to the XIS detectors has been reported to be 1.16 for the HXD nominal position and V1.2.2.3 data (Ishida et al. 2006), and we use this value in the following analysis.

Fig. 5 shows the entire 0.7–40 keV spectrum as a ratio to the simple phenomenological 2–10 keV model discussed in Section 3.1. In addition to the soft excess we see clear excess emission in the PIN detector. In order to check if this emission can be reproduced by the Compton hump of our 0.7–10 keV two-reflector model we extrapolate this model to 40 keV. This gives χ^2/d.o.f. = 5690/5410 for the entire 0.7–40 keV band. Fitting of the model with the PIN data included does not improve the quality of the fit or change any of the parameter values. The fit is shown in Fig. 6 and we see that the model slightly underpredicts the PIN data. Given that the source is not very bright in the hard X-rays, this slight discrepancy is likely to be due to uncertainties in the background models (both non-X-ray background and the CXB) and/or the cross-normalization of the PIN with respect to the XIS detectors. If we instead extrapolate the blurred absorption model to include the PIN data, we get χ^2/d.o.f. = 5734/5410, i.e. $\Delta\chi^2 = 43$ worse than for the two-reflector model. Fitting of the absorption model with the PIN data included results in a slightly higher contribution from the reflector, which improves the quality of the fit by $\Delta\chi^2 = 4$. The high-energy data
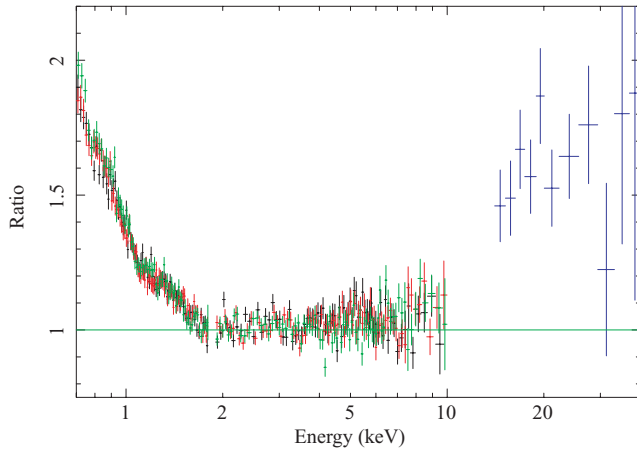
Figure 5. The broad-band *Suzaku* spectrum of Mrk 335 shown as a ratio to the simple 2–10 keV power-law + Gaussian model. Excess emission is clearly visible both at low and high energies. Data from the three FI XIS are shown in black, red and green. The PIN data are shown in blue.
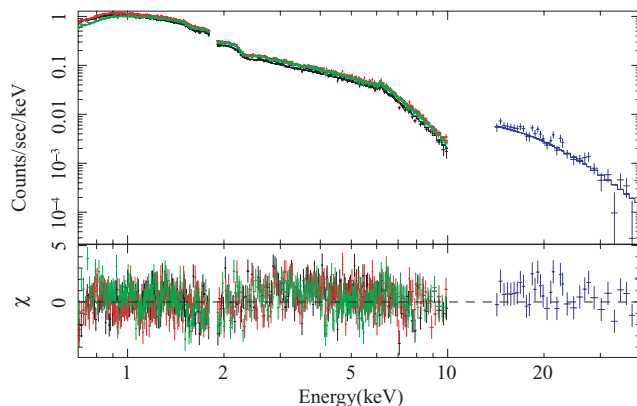

Figure 6. The broad-band *Suzaku* spectrum of Mrk 335. The upper panel shows the data together with the two-reflector model shown in Fig. 3. The lower panel shows the residuals of the fit. Data from the three FI XIS are shown in black, red and green. The PIN data are shown in blue.

hence favour the two-reflector model, although both models are acceptable given the uncertainties mentioned above.

4 THE TIME-AVERAGED *XMM–Newton* SPECTRUM

Mrk 335 was observed for 133 ks by *XMM–Newton* about six months before the *Suzaku* observation, and a comparison between these two observations is likely to provide interesting information about the source. Because *XMM–Newton* is more reliably calibrated at low energies, we also expect that the *XMM–Newton* data will allow us to put better constraints on the two-reflector model at low energies.

We start, however, by considering the 2–10 keV time-averaged spectrum. The most notable difference compared to the *Suzaku* data in this energy range is the very clearly double-peaked Fe line profile, shown in Fig. 7. Detailed fitting of the line profile has been presented by O'Neill et al. (2007), who find that a moderately broad relativistic line is present but that the two peaks at 6.4 and 7 keV are most likely due to narrow lines, identified with Fe Kα and Fe XXVI Lyα, respectively. The two lines are suggested to originate in the molecular torus of AGN unification models, and in highly ionized
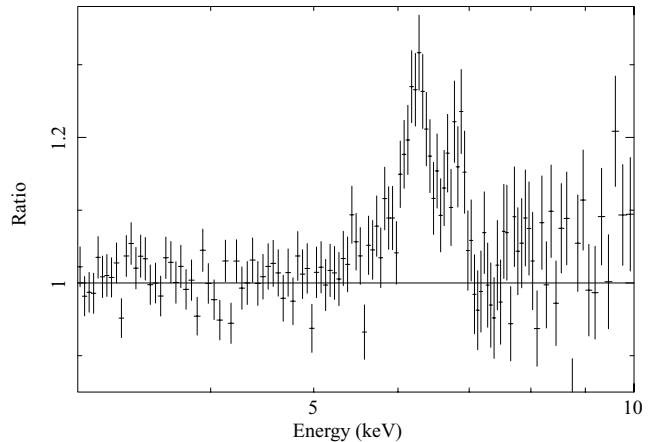

Figure 7. The *XMM–Newton* pn spectrum shown as a ratio to a power law fitted over the 3–4.5 and 7.5–10 keV energy ranges. The Fe line profile is clearly double peaked, but apart from the blue peak it is very similar to the profile shown in Fig. 1 for the *Suzaku* data.

gas filling this torus, respectively. Here we simply note that the Fe line profile can be fitted with the same model as the *Suzaku* data if a narrow line is added around 7 keV, in agreement with the findings of O'Neill et al. (2007).

With the addition of the narrow line around 7 keV, the entire 2–10 keV *XMM–Newton* spectrum can be very well fitted with the models presented for the *Suzaku* data. As an example, our model with reflection arising from outside $40r_g$ in a disc with $\xi = 30$ erg cm s^{-1}, gives χ^2/d.o.f. = 1324/1353, with the photon index and the relative normalization of the different components changing very little from the *Suzaku* values. For the two narrow lines we find energies of $6.41^{+0.02}_{-0.03}$ keV and $7.05^{+0.03}_{-0.05}$ keV, with EWs of 43 ± 13 eV and 32 ± 14 eV, respectively. The 2–10 keV flux determined from the model is 1.78×10^{-11} erg cm^{-2} s^{-1}, compared to 1.43×10^{-11} erg cm^{-2} s^{-1} for the *Suzaku* data. The flux in the narrow Fe Kα is consistent with not having changed between the observations, with $7.41^{+1.76}_{-1.53} \times 10^{-6}$ photons cm^{-2} s^{-1} obtained for *Suzaku* and $6.58^{+1.44}_{-1.99} \times 10^{-6}$ photons cm^{-2} s^{-1} for *XMM–Newton*.

At low energies, larger differences between the two data sets can be seen. In terms of the two-reflector model, much of this difference can be explained by increasing the ionization parameter of the inner reflector from about 300 erg cm s^{-1} to about 1200 erg cm s^{-1} (no solution with the same ionization parameter for the inner reflector in both data sets was found). However, in order to get a good fit all the way down to 0.4 keV we also need to include an edge at 0.51 keV with $\tau = 0.33$ (as for XIS1, possibly consistent with the 0.49 keV C VI edge). If we let all the parameters of the model vary we find a best-fitting 0.4–10 keV two-reflector (+ edge) model with χ^2/d.o.f. = 1749/1670. Apart from the higher ionization parameter for the inner reflector, the only parameters in this model that differ significantly from the *Suzaku* FI XIS fits are the photon index and the emissivity index. These are both steeper; $\Gamma = 2.28 \pm 0.01$ and $q = 5.9^{+0.4}_{-0.6}$, respectively (we froze q at 3 for the FI XIS data). The reflection fraction and relative contribution of the two reflectors in this model are very close to what we found for the *Suzaku* data.

5 SPECTRAL VARIABILITY

In Fig. 8, we show the 0.5–12 keV background-subtracted XIS3 light curve from the *Suzaku* observation of Mrk 335. The figure also defines the high and low states which we will use to study the
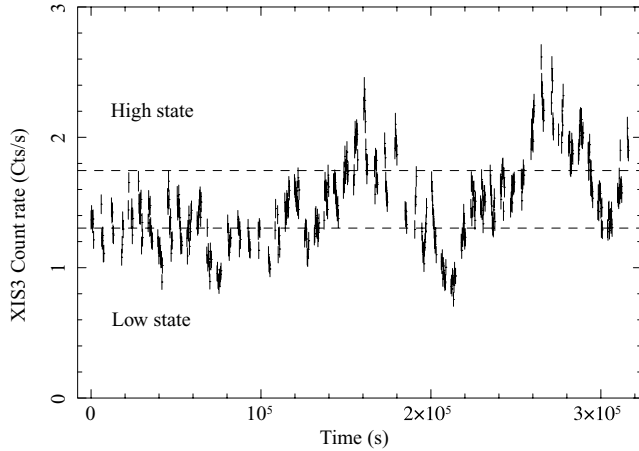
Figure 8. The XIS3 light curve in the 0.5–12 keV band in 300-s bins. We also show the high- and low-flux states, which were defined so that they have roughly the same number of counts.

Figure 10. The mean XIS hardness ratio (black, solid line) as a function of time together with the rescaled, mean XIS 0.5–12 keV light curve (red, dashed line). The source hardens significantly during the dips in the light curve but softens very little during the two big flares. The vertical dashed lines divide the observation into three time intervals of equal length. We will consider the rms spectra from these three intervals in Section 5.3.

spectral variability. The source varies by a factor of about 2.5 during the observation and the light curve notably contains two big flares.

Below, we will investigate the spectral variability of Mrk 335 during the *Suzaku* observation by considering hardness ratios, the high and low states, and rms spectra. Because of the high uncertainties in the PIN background on short time-scales we limit this analysis to the XIS data. At the end of the section we will compare our results with the variability properties of the *XMM–Newton* data.

5.1 Hardness ratios

As a first, model-independent way of characterizing the spectral variability of the source, we calculate hardness ratios, $HR = (H - S)/(H + S)$, where we take H to be the count rate in the 3–10 keV band and S to be the count rate in the 1–2 keV band. The mean XIS hardness ratio, calculated in orbital length bins of 5760 s, is plotted as a function of the mean $H + S$ count rate in Fig. 9. At low count rates there is a clear anticorrelation between the hardness ratio and the count rate, but this anticorrelation flattens out as the count rate increases. This curious behaviour is even more evident in Fig. 10,
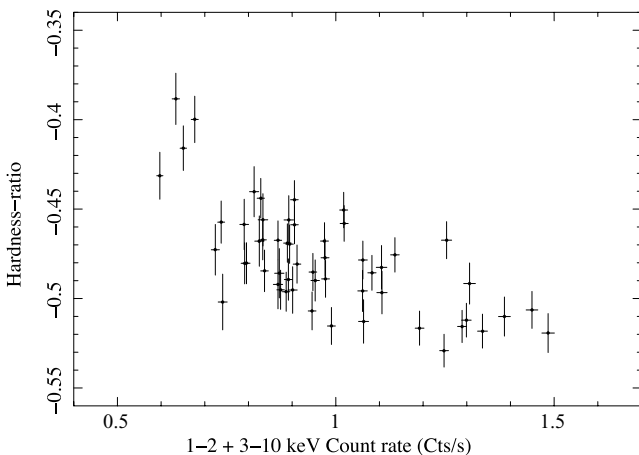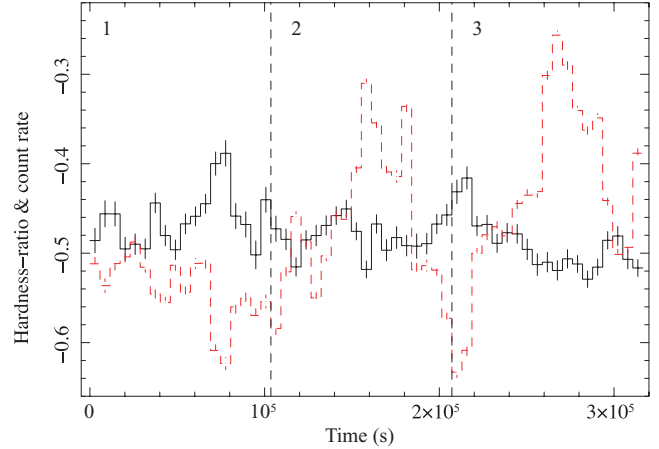
which shows the mean XIS hardness ratio as a function of time, together with the rescaled, mean XIS 0.5–12 keV light curve. We see that the source hardens significantly during the dips in the light curve but that it does not soften by a corresponding amount during the two big flares.

In Fig. 10, we also divide the observation into three time intervals of equal length. The hardness ratio in the middle part varies less than it does in the first and the third parts (mainly because this part of the light curve does not contain any large dip), and in Section 5.3 we will see how this leads to different shapes of the rms spectra for the three intervals.

5.2 High and low states

In the previous section we have seen that there is an anticorrelation between the spectral hardness and the flux of the source. In order to investigate what spectral component(s) is(are) responsible for this behaviour we now consider flux-selected spectra. We select low-, intermediate- and high-state FI XIS spectra as defined in Fig. 8. With these selection criteria, the high and low states have about the same number of counts, corresponding to one-fourth of the total number of counts each. We fit both a phenomenological model and the two-reflector model (described in Section 3.2) to each of the three states over the 0.7–10 keV energy band.

The phenomenological model consists of a power law, a blackbody to model the soft excess, and a broad and a narrow Gaussian line to model the broad and narrow components of the Fe line. We let all parameters vary apart from the widths of the Gaussian lines, which we freeze at $\sigma_{broad} = 0.47$ keV (as found for the time-averaged fits in Section 3.1) and $\sigma_{narrow} = 1$ eV. The results from the fits are presented in Table 1. As expected, we see clear evidence of spectral pivoting, with the photon index of the power law increasing from 2.07 in the low state, to 2.12 in the intermediate state, and 2.16 in the high state. (This linear increase of Γ is simply an effect of how the flux states were selected. When selecting a lower low state, we do indeed see a much harder power law, as expected from Figs 9 and 10.) The temperature of the blackbody is found to be roughly constant at 0.14 keV in all three states, while its normalization increases with flux. Since the luminosity of a blackbody should scale with its

Figure 9. The mean XIS hardness ratio as a function of the mean count rate. The hardness ratio is defined as $(H - S)/(H + S)$, where H is the count rate in the 3–10 keV band and S is the count rate in the 1–2 keV band. The source clearly hardens significantly at low count rates.

Table 1. Results from fits to low-, intermediate- and high-state FI XIS spectra over the 0.7–10 keV band. The upper values are for a simple phenomenological model and the lower values are for the two-reflector model described in Section 3.2.

Parameter		Low state	Intermediate state	High state
Power law + blackbody + broad line + narrow line				
Γ		2.07 ± 0.02	2.12 ± 0.02	2.16 ± 0.02
PL norm	$\times 10^{-3}$	$4.74^{+8.26}_{-0.10}$	6.42 ± 0.10	8.59 ± 0.20
BB temp	eV	134^{+2}_{-5}	135 ± 4	142^{+3}_{-4}
BB norm	$\times 10^{-4}$	$1.41^{+0.11}_{-0.10}$	$1.76^{+0.10}_{-0.09}$	$2.09^{+0.15}_{-0.14}$
E_{broad}	keV	$6.54^{+0.14}_{-0.11}$	$6.41^{+0.09}_{-0.08}$	$6.42^{+0.13}_{-0.12}$
EW_{broad}	eV	291^{+79}_{-74}	294^{+60}_{-57}	288^{+85}_{-79}
E_{narrow}	keV	6.36 ± 0.04	6.39 ± 0.05	$6.38^{+0.12}_{-0.10}$
$Flux_{narrow}$	$\times 10^{-6}\,ph\,cm^{-2}\,s^{-1}$	$5.43^{+3.87}_{-2.37}$	$3.19^{+3.10}_{-2.12}$	$5.04^{+4.65}_{-4.63}$
χ^2/d.o.f.		2818/2831	3870/3879	2693/2659
Power law + two reflectors + narrow line				
Γ		2.14 ± 0.02	2.20 ± 0.02	2.26 ± 0.02
PL/tot flux[a]	(0.7–10 keV)	0.72	0.74	0.75
Ref_{inner}/tot flux[a]	(0.7–10 keV)	0.22	0.19	0.18
Ref_{outer}/tot flux[a]	(0.7–10 keV)	0.06	0.07	0.07
E_{narrow}	keV	6.37 ± 0.03	6.38 ± 0.03	$6.37^{+0.07}_{-0.06}$
$Flux_{narrow}$	$\times 10^{-6}\,ph\,cm^{-2}\,s^{-1}$	$7.94^{+2.66}_{-2.44}$	$6.22^{+2.30}_{-2.13}$	$8.53^{+4.07}_{-4.00}$
χ^2/d.o.f.		2800/2833	3826/3881	2665/2661

[a]Error bars are not given as it is currently not possible to calculate errors on fluxes of specific model components in XSPEC.

temperature, this confirms that the soft excess is not really a black-body. For the broad component of the Fe line, we find that the EW stays nearly constant, showing that this component varies together with the continuum. The parameters of the narrow line are not very well constrained, but we note that the flux of the line is consistent with being constant, as would be expected if the line originates in distant material.

We next fit the three flux states with the two-reflector model from Section 3.2. We freeze all parameters apart from Γ, the energy of the narrow line, and the four normalizations (power law, two reflectors and narrow line) at the time-averaged values found in Section 3.2. The results from these fits are also presented in Table 1. As for the phenomenological model, the power law steepens with flux, with Γ increasing from 2.14 in the low state to 2.26 in the high state. Any attempts to fit the data with Γ frozen at the time-averaged value of 2.19 give fits which are significantly worse than those presented in the table.

As a measure of the relative contribution of the power law and the two reflectors in the different flux states, Table 1 gives the ratio of the flux in each of these components to the total 0.7–10 keV flux. We find that the outer reflector contributes by the same amount (6–7 per cent) in all the flux states, while the inner reflector contributes slightly more to the low state (22 per cent in the low state compared to 18 per cent in the high state), indicating that it is somewhat less variable. Although this effect is quite small, we note that a less variable inner reflector would be expected in a picture where light bending is important close to the central black hole (e.g. Miniutti & Fabian 2004).

Since the spectral hardening is most prominent in the two deep dips of the light curve we also extracted spectra in these intervals. Specifically, we selected the 12 ks (∼6-ks exposure) with the lowest count rate in each of the dips. The fits of these spectra are consistent with the trends discussed above, although the short exposure times

make it difficult to unambiguously disentangle the contribution from the different spectral components.

From the fits to both of the models presented above it seems clear that the main driver behind the observed anticorrelation between the hardness ratio and the flux is a pivoting power law. Both the broad Fe line and the soft excess appear to largely vary together with the continuum, while the narrow component of the Fe line is consistent with being constant.

5.3 rms spectra

Another way of gaining insight into the variability properties of Mrk 335 is the rms spectrum, which, for a given time-scale, shows the fractional variability as a function of energy. The techniques for calculating rms spectra are described in e.g. Edelson et al. (2002) and Vaughan et al. (2003).

Fig. 11 shows rms spectra of Mrk 335, calculated on the orbital time-scale of 5760 s. In order to investigate whether the rms spectrum changes with time, we have calculated rms spectra from the first, second and third parts of the observation (the three intervals are defined in Fig. 10) in addition to the rms spectrum of the entire observation. The errors from the Poisson noise were calculated following Vaughan et al. (2003).

The rms spectrum of the entire observation (black crosses in Fig. 11) peaks around 1 keV and then decreases with energy, a trend which is commonly observed in AGN. This behaviour is often explained either in terms of a pivoting power law, or in a model consisting of a constant reflection component and a power law that varies in normalization but not in shape. It can also be explained in an absorption model, assuming that the ionization parameter of the absorber is driven by the continuum variability (Gierliński & Done 2006). In the case of Mrk 335, the fits to the different flux states in the previous section suggest that the shape of its rms spectrum
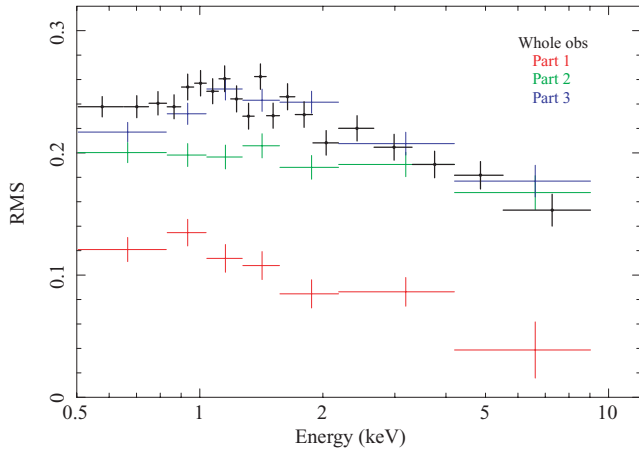
Figure 11. rms spectra of Mrk 335 on a 6 ks time-scale. The rms spectrum of the entire observation is shown in black, while rms spectra in red, green and blue were calculated for the first, second and third parts of the observation (as indicated in Fig. 10). The middle part of the observation clearly gives a much flatter rms, consistent with the small variation in hardness ratio seen in Fig. 10 during this time interval.

is mainly due to a pivoting power law, but that a somewhat less variable inner reflector may also contribute.

The rms spectra from the three parts of the observation show a change in shape as well as in normalization, with the middle part being significantly flatter than the first and the last parts, which both have roughly the same shape as the rms of the whole observation. The flatter rms of the middle part is consistent with Fig. 10, which shows that the hardness ratio is less variable during this period (the hardness only changes significantly during the large dips in the light curve, none of which are present during the middle part). The change of the shape of the rms spectrum is hence simply due to the position and the length of the time interval that is being probed, and does not imply that the source has entered a new mode of variability or changed its spectrum (the time-averaged spectra of the three time intervals are essentially identical). We also note that the flat shape of the rms is difficult to explain within the absorption model, which, assuming that the ionization state of the absorber responds to the variable continuum, predicts an enhanced variability in the 0.8–2 keV range (see also O'Neill et al. 2007).

In order to confirm that the two-reflector model is able to accurately describe the variability, we also produced synthetic rms spectra for the three intervals and the entire observation. This was done by fitting the model to the individual 6-ks spectra and then using the best-fitting models to extract fluxes in the different energy bands. We find a good match between the observed and synthetic rms spectra as long as we let the photon index and the normalizations of the three components be free parameters in the fits, as expected from the results of the previous section. Although this result is encouraging, it should be noted that this simply means that our two-reflector model provides a good fit to the entire energy range in all the individual time intervals.

5.4 Comparison with the *XMM–Newton* observation

In Section 4, we have seen that the long *XMM–Newton* observation of Mrk 335 catches the source in a very similar flux state as the *Suzaku* observation does six months later. The time-averaged spectra of the two observations are very similar above 2 keV (apart from an emission line at 7 keV only present in the *XMM–Newton* data),
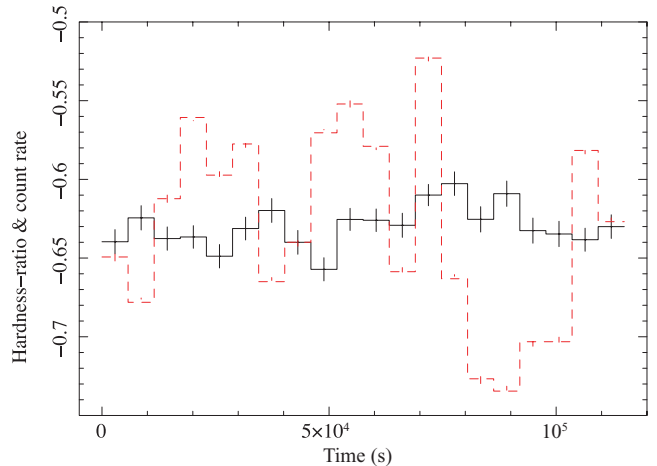

Figure 12. Same as Fig. 10, but for the *XMM–Newton* observation. Note that both the light curve (red, dashed line) and the hardness ratio (black, solid line) are much less variable than in the *Suzaku* observation.

and we find that similar two-reflector models fit both data sets also at lower energies. In this section we will extend the comparison between the two observations by considering some of the variability properties of the *XMM–Newton* data.

Fig. 12 shows the hardness ratio together with the rescaled light curve of the *XMM–Newton* observation, calculated in the same time bins as for the *Suzaku* observation (cf. Fig. 10). We note that both the count rate and the hardness ratio are much less variable than in the *Suzaku* observation, and that they do not show a correlation.

From the almost constant hardness ratio we would expect the rms spectrum of the *XMM–Newton* observation to be fairly flat. This is exactly what we see in Fig. 13, which shows the rms spectrum on both a 1 and 6 ks time-scale (the *Suzaku* rms spectra were calculated on a 6 ks time-scale). The 1 ks rms spectrum is consistent with being constant at 0.12, in excellent agreement with O'Neill et al. (2007). The 6 ks rms decreases slightly with energy, but is still much flatter than the rms spectrum of the entire *Suzaku* observation. This difference would naively suggest that the source has changed its behaviour dramatically in the six months between the two observations. However, we have seen that the *Suzaku* rms changes in shape during the observation, and that the curved shape arises when the light curve contains a large dip, in which the source hardens significantly. It therefore seems plausible that the rms spectrum is flat during the *XMM–Newton* observation simply because the count rate never drops to a low enough level. This interpretation is further supported by the fact that the flux is slightly higher in the *XMM–Newton* observation and that it is only a third as long as the *Suzaku* observation.

Fig. 13 also shows the 5–10 keV range of the 6 ks rms with a much finer energy binning, revealing a clear dip in the variability at 7 keV. This supports our interpretation that the 7-keV peak seen in the spectrum is a narrow line originating in distant material

6 DISCUSSION

Mrk 335 exhibits a strong soft excess below about 2 keV and does not show any signs of complex, warm absorption at low energies. This makes it an ideal target for studying the origin of the much debated soft excess.

In this paper we have focused on explanations for the soft excess which involve blurred reflection from an accretion disc. Such models
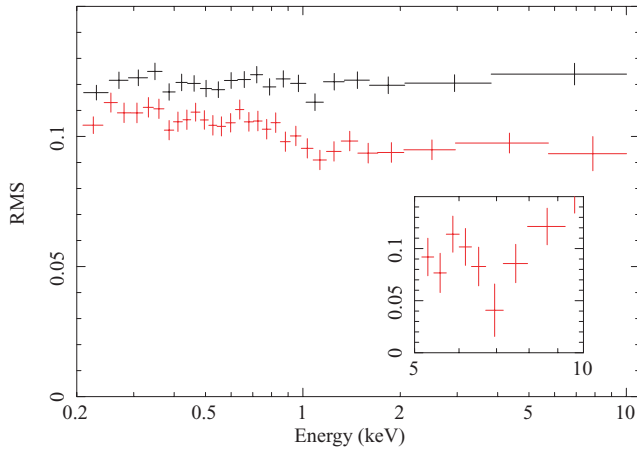
Figure 13. rms spectra of the entire *XMM–Newton* observation on a 1 ks (black) and a 6 ks (red) time-scale. The 1 ks rms is consistent with being constant at 0.12. The 6 ks rms decreases slightly with energy but it is much flatter than the rms of the whole *Suzaku* observation. The inset shows the 5–10 keV range of the 6 ks rms with a much finer energy binning. There is a clear dip in the variability at 7 keV, confirming that the 7-keV peak seen in the spectrum originates in distant material.

have been successful in fitting the spectra of previous observations of Mrk 335 (e.g. Ballantyne et al. 2001; Crummy et al. 2006). In the case of the recent *Suzaku* and *XMM–Newton* observations, we find that two reflectors are required in order to simultaneously explain the strong, smooth soft excess and the moderately broad Fe line. Our best-fitting model comprises a power law, an inner, heavily blurred, ionized reflector (which produces most of the soft excess) and an outer, almost neutral reflector (which is responsible for most of the Fe emission).

The requirement for more than one reflector is a consequence of several plausible disc/corona configurations. A power-law source in the form of a patchy corona, as well as a coronal geometry that changes with time (e.g. due to magnetic processes), would for instance give rise to different parts of the disc having different ionization states. However, about half of the reflected emission in our model originates outside about $40r_g$, which seems implausible for a disc with a patchy corona. A more centrally concentrated power-law source could produce such a situation if it, for example, consists of two sources at different heights, so that the inner and outer parts of the disc are predominantly irradiated by the lower and upper sources, respectively. Alternatively, the emission from a power-law source located very close to the black hole could be beamed along the disc (e.g. due to rotational motion about the black hole), which in combination with flaring of the disc at large radii would lead to a higher illumination of the outer disc. We also note that models with multiple reflectors have been successful in modelling the spectra of several other Seyfert 1 galaxies, e.g. 1H 0707−495 (Fabian et al. 2002) and PG 1211+143 (Crummy et al. 2006). It seems likely that such models could be important in other sources that, like Mrk 335, exhibit a strong soft excess in combination with a moderately broad Fe line.

It is important to note that our two-reflector model for Mrk 335 relies on the fact that the inner reflector with $\xi \approx 300$ erg cm^{-1} produces a very weak Fe line. This is because the majority of the Fe in this ionization state is in the form of L-shell ions, which in the REFLION model are assumed to produce very little Kα emission due to resonant Auger destruction. However, the amount of resonant Auger destruction depends on the conditions in the accretion disc,

and it is possible that the fluorescent yield for several Fe L-shell ions actually remain high (Liedahl 2005). It is not clear to what extent this would affect our conclusions.

It should also be noted that the reflection model used for the analysis in this paper assumes a constant density throughout the disc. It has been pointed out by Done & Nayakshin (2007) that the soft excess is much weaker if a hydrostatic model for the disc is used. This is because the partially ionized material that produces the soft excess can only exist in a thin layer in a hydrostatic disc. However, it is not at all clear that accretion discs are in hydrostatic equilibrium, as e.g. magnetic fields are likely to be important. This therefore does not pose a serious problem for the interpretation that the soft excess is due to reflection.

Our analysis of the spectral variability of Mrk 335 in terms of the two-reflector model shows evidence for a pivoting power law and suggests that both reflectors are varying together with the continuum (although there is some evidence that the inner reflector is slightly less variable). This behaviour is rather different from that observed in the typical flux states of many other reflection-dominated sources, such as MCG−6-30-15 (Miniutti et al. 2007), NGC 4051 (Ponti et al. 2006) and 1H 0707–495 (Fabian et al. 2004). In these sources the spectral variability can be described in terms of a power law that varies in normalization (but not in slope) and a much less variable reflection component. The spectral variability in Mrk 335 is also unusual in that the biggest changes occur in the low-flux states, where the source hardens substantially. The reason for this unusual behaviour is unclear and more data when the source is in a low state is needed in order to properly study this variability.

As an alternative to the reflection model we have also explored the possibility of the soft excess being produced as a result of smeared absorption. We have seen that the SWIND1 absorption model provides a very good fit to the spectrum of Mrk 335 as long as we only consider the data up to 10 keV. However, the model underpredicts the PIN data in the 14–40 keV range, suggesting that more reflection is present in the spectrum. The observed flat rms spectra of the *XMM–Newton* observation and part of the *Suzaku* observation also disagree with the absorption model, as this model predicts enhanced variability in the 0.8–2 keV range, assuming that the ionization state of the absorber responds to the changing luminosity of the source (Gierliński & Done 2006). As previously mentioned, the SWIND1 absorption model is also problematic in its simplistic treatment of the velocity field, and it seems like a more realistic model cannot produce the smooth shape of observed soft excesses unless extreme velocities are incorporated (Schurch & Done 2007). An absorption origin for the soft excess in Mrk 335 hence seems very unlikely.

We have seen that the shape of the hard spectrum of Mrk 335 can be very well explained with a blurred reflection model. However, it should be pointed out that partial covering models have also been seen to provide acceptable fits to the 3–10 keV energy band in e.g. the *XMM–Newton* observations of the source (Longinotti et al. 2007; O'Neill et al. 2007). We have not considered partial covering models in our analysis but we note that the rapid variability of Mrk 335 implies that the emission region must be very small (less than about 1 light-hour across), and a partial coverer would hence have to be even smaller and very dense. We also note that a broken power law (or some other additional component) is required to explain the soft excess within a partial covering model (Grupe et al. 2007), making such a model less physically plausible.

Our comparison of the *XMM–Newton* and *Suzaku* observations has provided interesting information about the origin of the narrow emission lines seen in this object. The 6.4-keV line is clearly detected in both observations and the flux in the line is consistent with

being constant, confirming that the line originates in distant material, e.g. the molecular torus of AGN unification models. The 7-keV line which is clearly seen in the *XMM–Newton* spectrum is, however, not detected in the *Suzaku* data. O'Neill et al. (2007) showed that the line cannot be attributed to the blue horn of the broad Fe line, and our own spectral and rms analysis support this interpretation. Specifically, our rms analysis shows that the line does not vary during the *XMM–Newton* observation, which places an inner limit on the origin of the line at about a light-day from the nucleus. On the other hand, the fact that the line has varied in the six months between the two observations places an outer limit on its origin at around a light-month. These constraints together suggest that the line originates somewhere in the broad-line region of the source.

7 SUMMARY

In this paper we have presented an analysis of a long *Suzaku* observation of the NLS1 galaxy Mrk 335. We have also considered a previous *XMM–Newton* observation of the source.

The *Suzaku* spectrum exhibits a broad Fe line and a strong soft excess, and does not show any signs of warm absorption, in agreement with previous observations. We find that a model consisting of a power law and two reflectors provides the best fit to the entire 0.5–40 keV time-averaged spectrum. In this model, a heavily blurred inner reflector produces most of the soft excess, while an outer reflector (outside $\sim 40 r_\mathrm{g}$) produces most of the Fe line emission.

The spectral variability of the *Suzaku* observation is characterized by spectral hardening at low count rates. Fitting of different flux states with the two-reflector + power-law model suggests that this hardening is mainly due to pivoting of the power law. The two reflectors appear to vary with the continuum, although there is some evidence for the inner reflector being less variable. The rms spectrum of the entire observation has the curved shape commonly observed in AGN, but the shape is significantly flatter when an interval which does not contain any deep dips in the light curve is considered. This suggests that the main driver behind the curved shape of the rms is the spectral hardening which occurs in these dips. The physical reason for this hardening is currently unclear.

The time-averaged *XMM–Newton* spectrum can be fitted with a similar two-reflector model as the *Suzaku* data and the two data sets have similar fluxes. However, the *XMM–Newton* data do not show a correlation between the spectral hardness and the count rate, and the rms spectrum is flat. Since the spectral hardening of the *Suzaku* data mainly occurs in the deep dips in the light curve, it seems plausible that the lack of significant spectral variability in the *XMM–Newton* observation is due to the fact that the count rate never drops to a low enough level.

We have discussed the implications of our findings for the origin of the soft excess in other Seyfert 1s, and we suggest that the two-reflector model might be applicable in other sources that show a soft excess which is stronger and/or smoother than expected from the Fe line properties. We have also noted that the observed flat rms spectra, as well as the high-energy data from the PIN detector, disfavour an absorption origin for the soft excess in Mrk 335.

REFERENCES

Ballantyne D. R., Iwasawa K., Fabian A. C., 2001, MNRAS, 323, 506
Bianchi S., Matt G., Haardt F., Maraschi L., Nicastro F., Perola G. C., Petrucci P. O., Piro L., 2001, A&A, 376, 77
Brenneman L. W., Reynolds C. S., 2006, ApJ, 652, 1028
Brenneman L. W., Reynolds C. S., Wilms J., Kaiser M. E., 2007, ApJ, 666, 817
Crummy J., Fabian A. C., Gallo L., Ross R. R., 2006, MNRAS, 365, 1067
Done C., Nayakshin S., 2007, MNRAS, 377, L59
Edelson R., Turner T. J., Pounds K., Vaughan S., Markowitz A., Marshall A., Dobbie P., Warwick R., 2002, ApJ, 568, 610
Fabian A. C., Ballantyne D. R., Merloni A., Vaughan S., Iwasawa K., Boller Th., 2002, MNRAS, 331, 35
Fabian A. C., Miniutti G., Gallo L., Boller Th., Tanaka Y., Vaughan S., Ross R. R., 2004, MNRAS, 353, 1071
George I. M., Turner T. J., Netzer H., Nandra K., Mushotzky R. F., Yaqoob T., 1998, ApJS, 114, 73
Gierliński M., Done C., 2004, MNRAS, 347, L7
Gierliński M., Done C., 2006, MNRAS, 371, L16
Gondoin P., Orr A., Lumb D., Santos-Lleo M., 2002, A&A, 388, 74
Grupe D., Komossa S., Gallo L., 2007, ApJ, 668, L111
Ishida M., XRT team, 2006, JX-ISAS-SUZAKU-MEMO-2006-40, 'Relative Normalizations of XIS and HXD-PIN for V1.2.2.3 Data'
Ishisaki Y. et al., 2007, PASJ, 59, 113
Laor A., 1991, ApJ, 376, 90
Liedahl D. A., 2005, in Smith R., ed., AIP Conf. Proc. Vol. 774, X-ray Diagnostics of Astrophysical Plasmas: Theory, Experiment and Observation. Am. Inst. Phys., New York, p. 99
Longinotti A. L., Sim S. A., Nandra K., Cappi M., 2007, MNRAS, 374, 237
Middleton M. J., Done C., Gierliński M., 2007, MNRAS, 381, 1426
Miniutti G., Fabian A. C., 2004, MNRAS, 349, 1435
Miniutti G. et al., 2007, PASJ, 59, 315
Nandra K., George I. M., Mushotzky R. F., Turner T. J., Yaqoob T., 1997, ApJ, 477, 602
O'Neill P., Nandra K., Cappi M., Longinotti A. L., Sim S. A., 2007, MNRAS, 381, L94
Ponti G., Miniutti G., Cappi M., Maraschi L., Fabian A. C., Iwasawa K., 2006, MNRAS, 368, 903
Pounds K. A., Stanger V. J., Turner T. J., King A. R., Czerny B., 1987, MNRAS, 224, 443
Reynolds C. S., 1997, MNRAS, 286, 513
Ross R. R., Fabian A. C., 2005, MNRAS, 358, 211
Schurch N. J., Done C., 2007, MNRAS, 381, 1413
Shakura N. I., Syunyaev R. A., 1973, A&A, 24, 337
Turner T. J., Pounds K. A., 1988, MNRAS, 232, 463
Turner T. J. et al., 1993, ApJ, 407, 556
Vaughan S., Edelson R., Warwick R. S., Uttley P., 2003, MNRAS, 345, 1271
Woo J., Urry C. M., 2002, ApJ, 579, 530

This paper has been typeset from a TeX/LaTeX file prepared by the author.